ReactorSTM : imaging catalysts under realistic conditions

Herbschleb, C.T.

Chapter 5

Hydrodesulphurization of thiophene

5.1 Hydrotreating: industry and research

The refinement of crude oil is one of the cornerstones of modern society. In this chemical process, the crude oil is converted into transportation fuels, such as gasoline and diesel oil. An important step in oil refining is the catalytic hydrotreating of liquid petroleum fractions, which are obtained after distillation of the crude oil. During catalytic hydrotreating, the hetero-atoms N, S, and O are removed from the petroleum fractions. During the combustion of the carbohydrates containing these elements, SO_2 and NO_x are formed, which are the main contributors to the formation of acid rain. Furthermore, these types of carbohydrates have a detrimental effect on the transition-metal based catalysts used in the further refining processes and in car exhausts. In addition, hydrotreating converts olefins and aromatics into saturated carbohydrates, which burn more cleanly (i.e. fully to CO_2 and H_2O). The annual sale of hydrotreating catalysts is 10% of the total global catalyst market, which emphasizes the importance of hydrotreating. In short, the hydrotreating catalyst consists of CoMo, NiMo, and NiW sulfides, dispersed on a highly porous γ-alumina support. CoMoS is the catalyst for desulphurization and NiMoS for denitrogenation and hydrogenation, and in one of the processes, NiWS assists in hydrocracking [140, 141].

Throughout the years, the hydrotreating catalysts have drastically improved, which is undoubtedly partly thanks to a contribution of scientific research. The main drive for this drastic improvement was legislation in the European Union and the United States. Up to now, European legislation

decreed six emission standards, starting from the end of the eighties to setting maxima to the emission of CO, NO_x, unburnt hydrocarbons, and soot, to improve the air quality [132][1]. Additionally, to decrease the SO_2 emission, the maximum sulphur content for fuel was decreed to be at maximum 350 ppm (diesel)/ 150 ppm (gasoline) from the year 2000, to 50 ppm from 2005, and to <10 ppm ("sulphur free") from 2009 onward. Although these standards have already been met, hydrodesulphurization, the hydrotreating process in which sulphur is removed from hydrocarbons, is still gaining a lot of attention, for various reasons. Firstly, to meet this ultra low sulphur standard, *deep desulphurization* of liquid petroleum fractions is necessary. Crude oil contains a large variety of organosulphur compounds, including thiols (R-S), sulfides (R-S-R), and aromatic heterocycles called thiophenes [133]. Within the group of thiophenes, the larger molecules, such as, for instance, 4,6-dimethyldibenzothiophene ($C_{12}H_8S$), are the real challenge to desulphurize, because they exhibit steric hindrance with respect to the active sites of the catalyst [134, 135], decreasing their reactivity towards desulphurization, as is illustrated in figure 5.1. Deep desulphurization means to desulphurize these types of molecules. With an increasing demand for light fuels such as diesel, refineries have increased their production of these fuels by cracking increasingly heavy feedstocks, which contain more of these large thiophenes. In addition, oil fields at different geological locations differ in sulphur content, which can be up to 5% in weight[2]; new oil fields, to be exploited in the future, are foreseen to contain, on average, more sulphur. Secondly, the reaction mechanisms for all hydrotreating catalysts are believed to be quite similar, since their structure is more or less the same. Legal standards for NO_x emission are still being intensified, meaning that the hydrodenitrogenation catalyst is still under pressure for improvement. Understanding the hydrodesulphurization reaction also assists improvement of the hydrodenitrogenation catalyst. And the economics of the hydrodesulphurization

[1]Euro 6, which should be met in 2014, sets the following emission standards for diesel and gasoline passenger cars (in g/km). Light commercial vehicles have similar standards [132].

	CO	HC	HC+NO_x	NO_x	PM
Diesel	0.5	-	0.17	0.08	0.005
Gasoline	1.0	0.10	-	0.06	0.005

[2]Five examples of crude oil from different geological orientations, in combination with their sulphur content (low sulphur content is "sweet" oil; high sulphur content is "sour" oil) are [136–138]:

Oil type	S content
West Texas Intermediate	0.24%
Brent Blend	0.37%
Dubai Crude (Fateh)	2%
Tia Juana heavy	2.82%
Boscan	5.4%

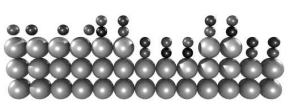

play a role in catalysis development. Currently, a typical plant heats a feedstock, mixed with a high amount of hydrogen (50-100 bar), to a temperature between 300℃ and 400℃, after which it is exposed to a fixed-bed reactor, containing highly dispersed catalytic nano-particles supported on γ-alumina. The exact combination of temperature and pressure depends on the sulphur content of the crude oil. Generally, the high temperature is needed to break the strong S-bonds, whereas the high hydrogen pressure is needed to prevent the catalyst from sulphur saturation. Hydrogen is expensive, and elevated temperatures cause the catalyst to age more quickly by coking and sintering – fundamental insights into the action of the catalyst might lead to lower operational temperatures and pressures [139–144].

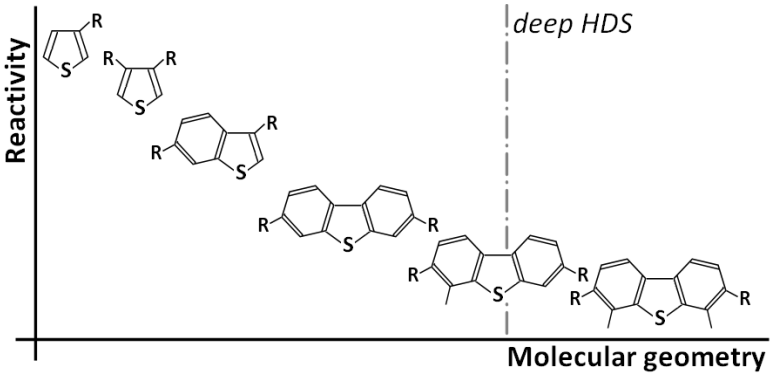

Figure 5.1: Various thiophene components which can be found in crude oil. The larger molecules are more difficult to desulphurize, because of steric hindrance [134, 135].

5.1.1 Catalyst structure and reactivity: Literature

The development of the high-quality catalyst used in today's desulphurization plants, molybdenum disulphide nano-crystallites, with cobalt as a promoter, was supported by extensive scientific research on this catalytic system. Direct and indirect insights into the structure and activity were gained by experimental studies, including gas chromatography [147], low energy electron diffraction (LEED) [148], Auger electron spectroscopy (AES) [148], STM [149–154], X-Ray crystallography [155], elastic scattering quantum chemistry, extended X-ray adsorption fine-structure spectroscopy (EXAFS) [156], and scanning electron microscopy; theoretical studies include electronic structure calculations [157–159, 164–166]. In these research efforts, both the non-promoted and the cobalt-promoted MoS_2 crystallites have been investigated.

Amongst the most important findings were the active sites of the catalyst: the edges, rims, and corners of the crystallites. In contrast, the basal planes exhibit no reactivity. Steps in the activated reaction cycle include the binding of reactants and reaction intermediates to the rims and sulphur vacancies in the edges; the formation of sulphur vacancies at the edges is favored, since the sulphur atoms are less strongly bound there, with respect to the ones in the basal plane. In addition, edge and rim positions provide a better accessibility to the large organosulphur compounds than the plane. Additional evidence for the activity of the edges and rims is an experimental study, which has shown a direct proportional relation between the amount of edge and rim sites on a sample containing MoS_2 nano-crystallites and its reactivity. The number of edge and rim sites can be decreased by sintering the crystallites into bigger particles. The promoters of the catalyst, cobalt, and nickel, are believed to replace molybdenum atoms at the edges of the crystallites, lowering the activation energy of, for example, the creation of a sulphur vacancy [173]. They also lower the activation energy for binding organosulphur molecules to the basal planes of the nano-particles, after which the additives assist diffusion of these molecules to the active sites [151]. The morphology of the MoS_2 crystallites, which determines the number of active sites, is an important issue, which depends on the reaction conditions. There have been many efforts to determine the composition, electronic structure, and morphology of MoS_2 nano-crystallites, in order to gain insight into the mechanisms behind the activity and selectivity of the catalyst. Extensive reviews on this subject exist in the literature [134, 140, 155, 171–174, 177]. This will be discussed in more detail below. The reaction mechanism has been investigated by studying hydrogen and thiophene interaction; thiophene desulphurises rather easily. Langmuir-Hinshelwood kinetics are accepted to be the mechanism for this reaction [155]. Apart from desulphurization, several hydrogenation steps take place on the surface of the catalyst; the various reaction pathways, in combination with the state of the edges under various conditions, have been studied extensively by DFT, and are supported by ex situ STM studies [145, 153, 175–177]. These will also be described in more detail in the paragraphs below.

Usually, unpromoted MoS_2 is used as a starting point for models of the hydrodesulphurization catalyst, since in situ EXAFS has shown that the catalysts used ordinarily consist of MoS_2 crystallites, with a size of 10 to 20 Å, after sulphidation at 300 to 400℃ [182]. Several STM studies have resolved these nano-particles atomically, providing valuable information about their morphology and edge terminations [142, 145, 153]. Figure 5.2 shows the basic structure of MoS_2. The crystallites consist of layered S-Mo-S slabs,

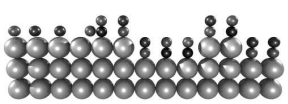

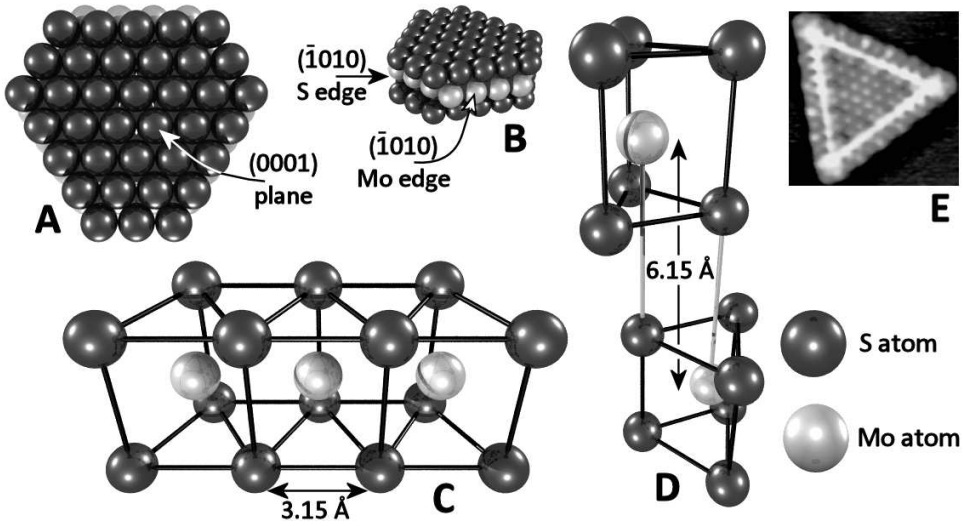

Figure 5.2: (A) A top view of a MoS_2 crystallite under reaction conditions; in this case the shape is a deformed hexagon [164, 178], rather than a triangle, as is the case under UHV or H_2S rich conditions [145]. The (0001) plane is indicated. (B) A 3D rendition of a MoS_2 crystallite, showing two possible edge terminations: a ($\bar{1}010$) S edge and a ($\bar{1}010$) Mo edge. (C) A side view of a single layer S-Mo-S slab; the atoms are hexagonally arranged. The interatomic distance is 3.15 Å[183]. (D) A unit cell of 2H-MoS_2. The Mo-Mo distance between the two layers is 6.15 Å[183]. (E) An STM image obtained by Helveg et al. [145] resolving a triangular MoS_2 crystallite on Au(111). A bright rim following the perimeter of the crystallite can be distinguished.

in which the atoms are arranged hexagonally in (0001) planes. In both the sulphur layers and the molybdenum layer, the interatomic distance is 3.15 Å. The molybdenum layer is trigonal-prismatically oriented with respect to the sulphur layers above and below, which span 3.16 Å, the thickness of a single MoS_2 slab. Multiple slabs are stacked in the same way as graphite, and are held together by Van der Waals interactions. Since this interaction is weak, one of the uses of MoS_2 is that of a lubricant. In molybdenite, the natural form of MoS_2, the second row is shifted by half, with respect to the first layer, creating a unit cell as depicted in figure 5.2 D. Here the distance between the two metal layers is 6.15 Å. STM images from earlier work have revealed a bright rim of high electron density, which follows the perimeter of the crystallites. This is attributed to the existence of localized electronic states on the edges. An example from the work of Helveg et al. [145] is shown in figure 5.2 E, illustrating this bright rim. Their studies concluded that the edge states are one-dimensional, localized perpendicular to the edges, but

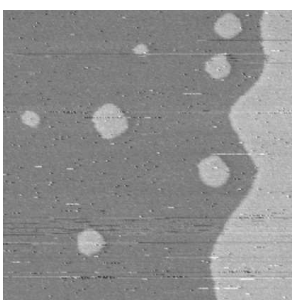

delocalized parallel to the edges [140, 143, 145, 171, 184, 185].

As can be seen in figure 5.2 B, there are two natural edge terminations: an $(\bar{1}010)$ S edge and an $(\bar{1}010)$ Mo edge. Initially, after preparing the MoS_2 crystallites under high sulphiding conditions ($p_{H_2S} \gg p_{H_2}$), previous STM studies in ultrahigh vacuum have shown that the crystallites exhibit a triangular structure, with the bright rim along the edges, as shown in figure 5.2 E. The triangular structure indicates that, under these conditions, one of the edges is favored above the other. By combining DFT studies with the STM results obtained, it was determined to be the $(\bar{1}010)$ Mo edge, in which the uncoordinated molybdenum atoms at the edges are decorated with sulphur dimers (fig. 5.3 C). Figure 5.3 B shows a different possible Mo edge termination, occurring under different environmental conditions: the 50% S covered Mo edge. Figure 5.3 A shows the bare Mo edge as reference. The bright rim is believed to correspond to metallic states occurring at the Mo edges of the crystallites, which in itself is a semiconductor [145, 153, 158–160]. The bright rim is believed to play a key role in the reaction mechanism, to be discussed below. The Mo edge is not, however, always the most stable configuration: there is a size effect [175]. An S:Mo ratio in the crystallites larger than approximately 3:1 seems to be energetically disfavored, leading to morphological transitions of the crystallites to lower the S:Mo ratio. This happens for small clusters, where the number of atoms along the edge $n \leq 6$, in which the sulphur excess relative to the bulk is relatively large with respect to Mo edges, which are decorated with sulphur dimers. The change in configuration for the smaller particles translates into triangular crystallites, exhibiting the $(\bar{1}010)$ S edges instead of the Mo edges. For even smaller clusters, the S edges undergo a transition from fully sulphided to 75% S coverage [175]. Since the Mo edge differs from the S edge, this size effect is predicted to have an influence on the reactivity of the catalyst. In the STM studies mentioned, two types of crystallites were distinguished, defined as type I and type II crystallites. Type I crystallites consist of single slabs of MoS_2, whereas type II crystallites comprise multiple MoS_2 slabs. At annealing temperatures T_a (see section 5.2), during preparation below 673 K, only type I crystallites are formed, whereas at higher T_a, also type II crystallites have been observed [145]. Another effect, observed at higher temperatures, is the sintering of smaller crystallites into larger ones, which accumulate at the steps on the Au(111) substrate [142].

When the crystallites are prepared under more reducing conditions, i.e. a larger $p_{H_2} : p_{H_2S}$ ratio, deformed hexagonal crystallites are obtained, along with rhombic, trapezoid, and pentagonal structures [145]. In our case, the

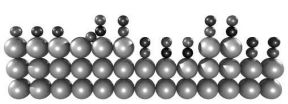

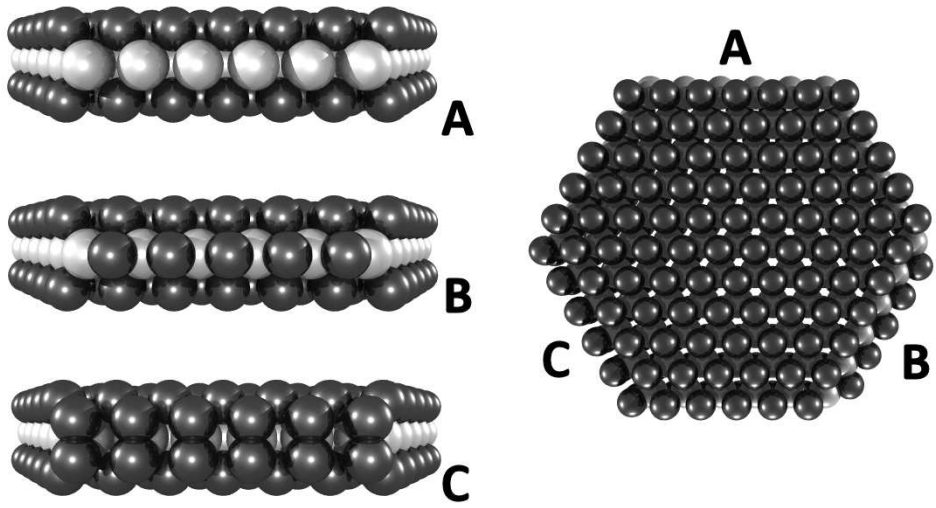

Figure 5.3: (A) A bare molybdenum edge, (B) sulphur monomers bonded to the molybdenum edge, (C) Sulphur dimers bonded to the molybdenum edge.

crystallites were deposited under sulphiding conditions, after which they were exposed to hydrogen, a reducing environment, in the reactor. Both the presence of the Mo edge, and the S edge were observed, as will be shown in section 5.4, probably in combination with adsorbed hydrogen. This indicates that, under more practical conditions, both edge terminations are present. The molybdenum edge is accompanied by the bright rim, which, to rule out support effects, is also observed when MoS_2 is deposited on carbon supports [177]. On the S edge, sulphur vacancies are created, when exposed to hydrogen; vacancy creation is also observed at the Mo edges, but only with pre-dissociated hydrogen at high temperatures [175]. The conversion of thiophenes, in particular the sterically hindered group of dibenzothiophenes, in the HDS process, mainly takes place via a pre-hydrogenation (HYD) route, rather than a direct desulphurization (DDS) route [179]. The edge terminations of the hexagonal crystallites, under HDS conditions, is predicted by DFT to consist of both Mo and S edges, with dissociated adsorbed hydrogen forming S-H groups. More specifically: (1) Mo edges with 50% S coverage, and 50% H adsorption, and (2) S edges, with 100% S coverage[3] and 100% H adsorption [160, 177, 180, 181], which is schematically depicted in figure 5.4.

Due to the various possible active edge sites, which act as adsorption sites, H donors, and activate C-S scission, there are numerous reaction pathways for thiophene to react to butene or butane. The process includes various

[3]which, under the influence of hydrogen, will also contain sulphur vacancies

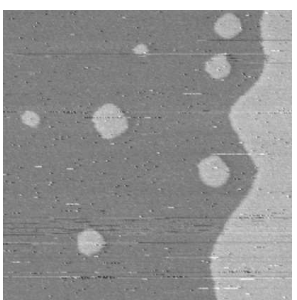

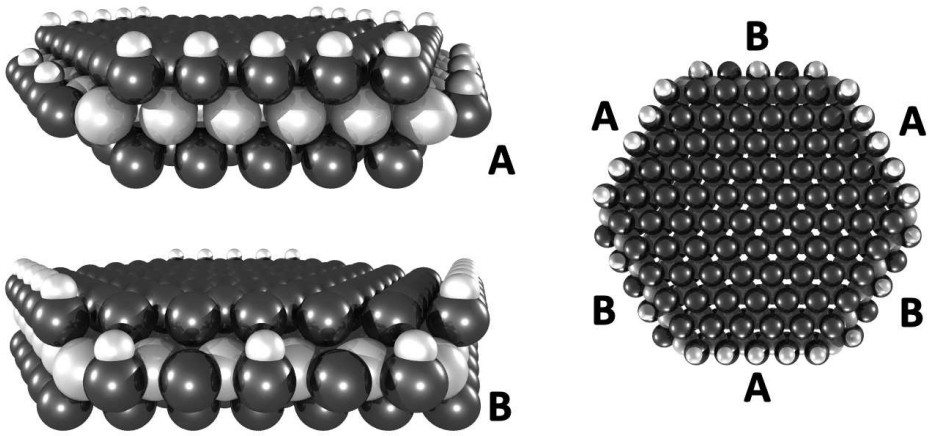

Figure 5.4: The edge termination of a MoS_2 crystallite under HDS conditions. Left: (A) An S edge, with 100% S coverage and 100% H adsorption; (B) An Mo edge, with 50% S coverage (S monomers) and 50% H adsorption. Right: Top view of the crystallite

hydrogenation steps, and a pre-hydrogenation step. The most recent reaction scheme is depicted in figure 5.5, adapted from reference [176]. The grey arrows represent very slow reactions. The top part shows the reaction intermediates on the sulphur edge, whereas the bottom part shows the reaction intermediates on the brim ("bright rim") sites of the molybdenum edge. The reaction scheme, in combination with the energy barrier calculations, give a few interesting predictions. Firstly, thiophene is found to prefer adsorption on the brim sites, whereas some of the reaction intermediates (e.g. 2,5-dihydrothiophene and cis-2-butenethiol) prefer to adsorb at a vacancy site on the S edge. Hydrogenation and H-transfer are favored on the brim sites, whereas C-S scission can occur on both the brim sites at the molybdenum edge, and the sulphur vacancy sites at the sulphur edge. The preferential site depends on the reaction conditions; under reducing conditions, C-S scission at the, in that case easily formed, S vacancies is favorable. Since desorption and diffusion of the reaction intermediates is fairly easy, the reaction mechanism under HDS conditions could be adsorption and pre-hydrogenation of thiophene at the brim sites, followed by diffusion to a vacancy site, where C-S scission takes place. A final important consideration is the regeneration of the active sites, which has a higher barrier at the S edge [143, 160, 176].

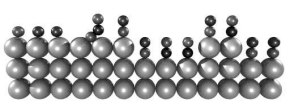

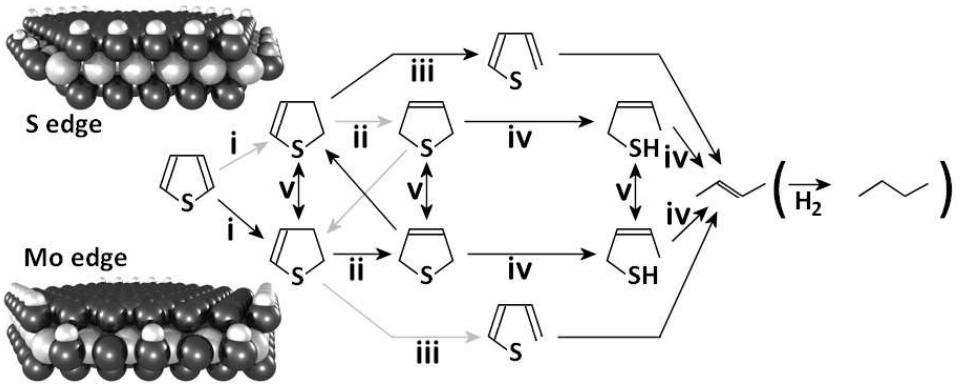

Figure 5.5: A schematic reaction scheme for the desulphurization of thiophene on either of the two edges, as defined in figure 5.4 under HDS conditions. The top part represents the S edge (vacancy model), whereas the bottom part represents the Mo edge (brim site model). (i) adsorption and pre-hydrogenation, (ii) hydrogenation, (iii) C-S scission (direct desulphurization), (iv) C-S scission in combination with hydrogenation, (v) diffusion. Grey arrows represent slow reactions [146, 176].

5.1.2 Enabling MoS_2 STM studies

When studying catalysis with STM, generally a well-prepared flat single crystal surface of the catalytic active material is used, which then is exposed to the particular reactants. In this case, however, one of the areas of interest is the morphological dynamics of MoS_2 nano-crystals under various conditions. Using a single MoS_2 crystal would be futile. A recipe for dispersing MoS_2 nano-crystallites on a conducting and chemically inert surface has been developed for STM studies on this reaction system – in short, molybdenum is evaporated onto the (111) surface of gold, in the presence of an excess of H_2S gas [145, 153]. Next to the inertness of bulk gold[4], the herringbone reconstruction onto its (111) surface provides good nucleation sites for highly dispersed metal islands [145]. In performing STM on the nano-crystallites, the bias voltage applied between tip and sample influence the apparent height of the crystallites. At increasing bias voltages, the apparent height asymptotically approaches the expected height for a single MoS_2 slab, 3.15 Å, whereas for small bias voltages, the apparent height goes to zero [153]. On the other hand, the distance between sample and tip also determines whether the current tunnels via the top sulphur layer (large distance), or directly to the molybdenum layer below (small distance). STM images in these two cases,

[4]Gold *nano*-particles are actually found to be catalytically very active for reactions such as CO oxidation [31–33]

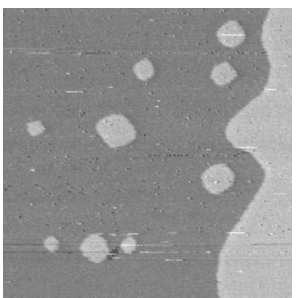

however, are reported to be quite similar, which makes it difficult, for example, to identify an S site on the surface [150].

5.1.3 MoS_2 catalysis in the ReactorSTM

The aim of this work was to study thiophene desulphurization in situ, under reaction conditions, with the ReactorSTM^{TM}, in order to investigate the influence of the conditions on the morphology of the crystallites. This included witnessing various steps in the reaction mechanism in situ, such as the binding of a thiophene molecule to a rim site, its conversion to reaction intermediates like thiolates, the creation of sulphur vacancies on the edges, and reaction of the intermediate species at these vacancies. To achieve this, the aforementioned recipe of depositing MoS_2 on Au(111) was used, and the surface was exposed at elevated temperatures to various mixtures of thiophene, hydrogen, and argon, at ambient pressures. The overall reaction studied is $C_4H_4S + 4H_2 \rightleftharpoons C_4H_{10} + H_2S$. Since both in preparing the catalyst, and performing the experiment, substances had to be used which are not commonly used with ultrahigh vacuum equipment (H_2S and thiophene), this was first performed as a pilot experiment on the ReactorSTM^{TM} Mark I, after some system adjustments. Then, the experiment was moved to the ReactorSTM^{TM} Mark II, described in detail in chapter 2[5].

5.2 Preparation

5.2.1 Setup adjustments

In order to make the ReactorSTM^{TM} compatible with the desulphurization experiment, adjustments had to be made at two fronts. Firstly, additions to the preparation chamber of the UHV system were necessary, and secondly, adjustments to the gas cabinet and the STM itself had to be made, to be able to run the experiment. Both will be discussed in this section.

To form the MoS_2 nano-particles, molybdenum is deposited on the surface, by electron beam deposition, in an H_2S background. For the molybdenum deposition, an E-beam evaporator [68] was installed on the UHV chamber, in combination with a quartz microbalance [167], for monitoring the deposition rate. H_2S was supplied to the chamber via a standard leak

[5]This work has been done in the framework of NIMIC [57], in cooperation with the company Albemarle Catalysts BV.

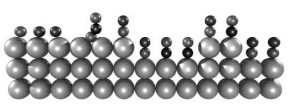

valve. The tubing, valves, and rotary pump [168] for the H_2S gas supply system, are all corrosion resistant.

Because one of the reactants, thiophene, is a liquid at room temperature (T_b = 84℃), the existing gas cabinet and parts of the ReactorSTM^{TM} had to be adapted, in order to offer gaseous thiophene to the MoS_2 catalyst, and to prevent thiophene from condensing in the gas lines and reactor[6]. Furthermore, clogging of the mass flow controllers, pressure regulators, and pumps had to be prevented. Figure 5.6 shows a schematic drawing of the modifications applied to the system.

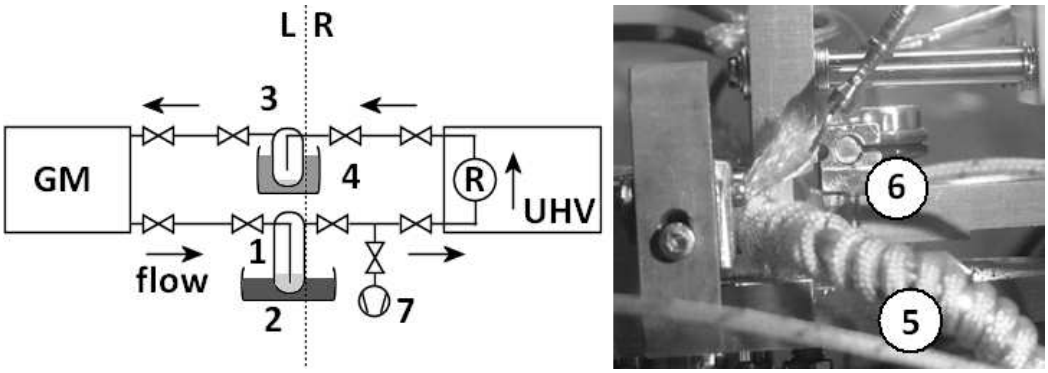

Figure 5.6: (Left) A schematic drawing of the modifications applied to the gas lines and ReactorSTM^{TM}. Left (L) of the dashed line, the equipment is at room temperature, while right (R) from the dashed line, all equipment is heated. (GM) The gas manifold, (1) thiophene flask, (2) heat bath, (3) cold trap, (4) ice bath, (R) reactor, (7) rotary pump. (Right) A detail photograph of the ReactorSTM^{TM}, showing the heated gas lines (5) and the cartridge heater heating the reactor (6).

Figure 5.6 schematically shows the flow path from the gas manifold (GM), via the reactor (R), back to the gas cabinet. The gas manifold supplies a mixture of argon and hydrogen, which bubbles through a flask containing thiophene (1), after which it enters a teflon tube. It is possible to heat up the thiophene, via a heat bath (2), in order to control the vapor pressure of thiophene. This opens the possibility of changing the amount of thiophene

[6]The modifications were only prepared for the gas cabinet and parts of the ReactorSTM^{TM} Mark I, which is discussed in this section. For the experiments performed in the ReactorSTM^{TM} Mark II, a separate gas cabinet was constructed, and during experiments, the whole STM chamber was heated to 120℃, in order to prevent C_4H_4S from condensing in the chamber or reactor.

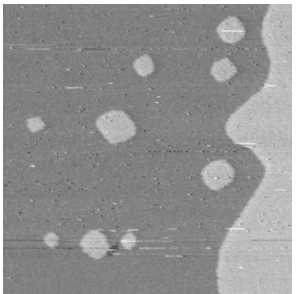

offered to the catalyst. To the right of the dashed line in the schematic, all components are heated. The gas lines outside the UHV are heated by heating tapes [65], while the gas lines inside the vacuum system are heated by a high resistance Cu alloy wire ($R = 6.8\ \Omega/\mathrm{m}$) (5). The reactor is heated by a cartridge heater (6) [169], clamped in a copper block, in order to create good thermal contact between the heater and the reactor. Both systems are equipped with separate thermocouples, for accurate temperature monitoring. A rotary pump (7) was added to the inlet, to be able to pump down the reactor, in case of a severe leak of the reactor. At the end of the heated gas line, a cold trap (3), cooled by an ice bath (4), was installed, to liquify the thiophene in the exhaust line, before the exhaust continues to the gas cabinet.

5.2.2 Sample preparation

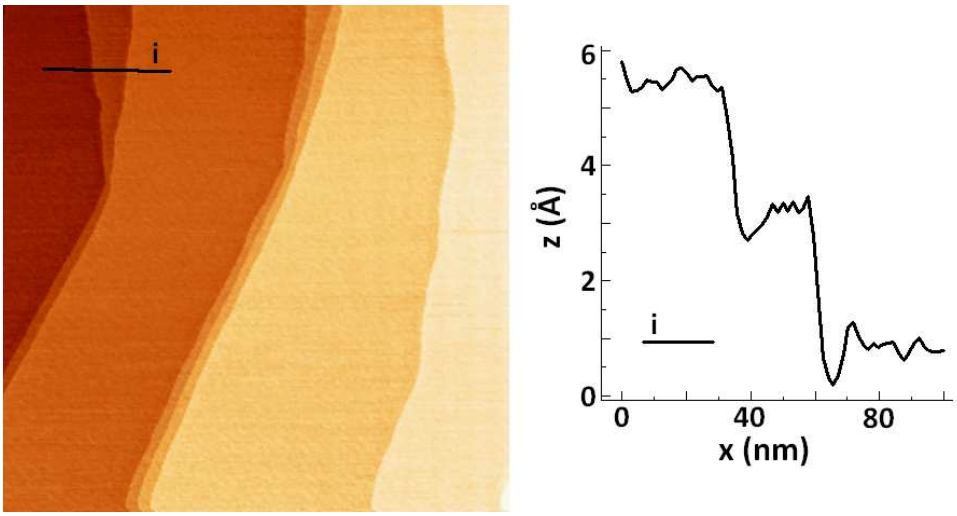

Figure 5.7: (Left) 400x400 nm^2 STM image (V_b = 80 mV; I_t = 0.2 nA), showing the clean Au(111) surface exhibiting large terraces. (Right) A height profile (i), showing the monatomic step height on Au(111) to be 2.3 Å.

As described in section 5.1, a gold surface, cut in the (111) direction, was chosen as a good support for MoS_2 nano-particles. First, the gold surface was cleaned by repeated cycles of 0.6 kV Ar^+ ion bombardment and annealing under UHV at 850 K. Figure 5.7 shows the surface of the prepared gold sample, which we used as a support for growing the MoS_2 crystallites. STM images obtained in the hours following this image show little variation, indicating that the surface is very stable; the height profile, in figure 5.7,

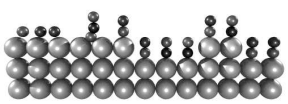

shows the monatomic step height of Au(111) to be 2.3 Å, which is well in accordance with the theoretical value of 2.36 Å [170].

Before creating the nano-particles, the cleanliness of the gold crystal was checked by LEED/Auger and STM. The procedure of creating the nano-particles, following the cleaning of the gold sample, is schematically depicted in figure 5.8.

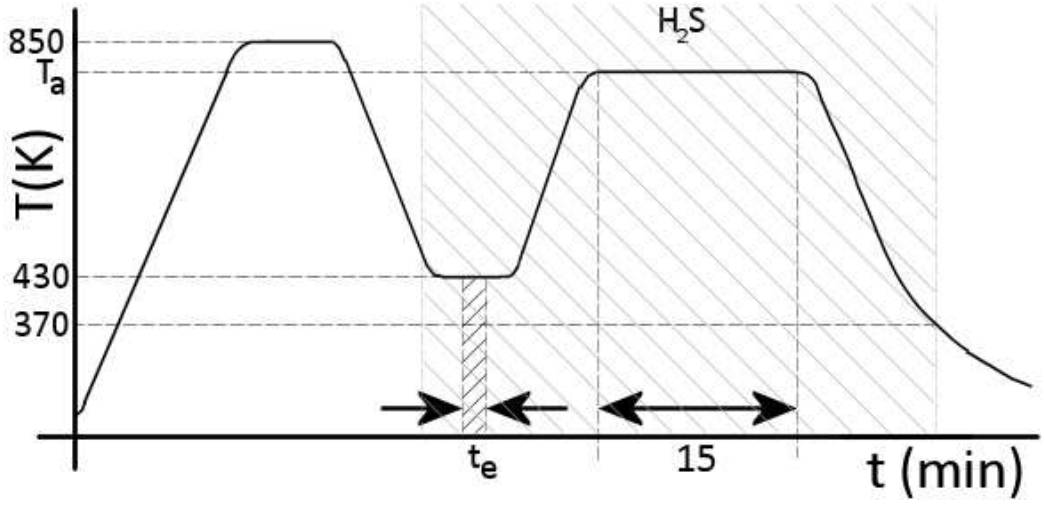

Figure 5.8: The graph shows the temperature evolution of the sample during the MoS_2 nano-particles preparation on Au(111) [142]. T_a represents the temperature at which the sample is annealed during H_2S exposure, after the evaporation of molybdenum. t_e is the duration of molybdenum evaporation. It is tuned such, that a coverage of 15 – 20% molybdenum is obtained.

Figure 5.8 starts with the final annealing step of the Au(111) surface at 850 K, after which the sample is cooled down to 430 K, which temperature is maintained. At this point, the UHV chamber is backfilled with H_2S, at a pressure of $1 \cdot 10^{-6}$ mbar. This is done because an excess amount of sulfur should be offered to the surface, in order to form MoS_2; backfilling the UHV chamber with $1 \cdot 10^{-6}$ mbar of H_2S corresponds to one monolayer of H_2S exposure to the surface per second. The evaporation time t_e is chosen such, that a coverage of 15 to 20 % MoS_2 nano-particles is obtained in the end; at a molybdenum flux of 70 nA, $t_e \approx 20$ seconds. After deposition, the sample is annealed for 15 minutes at temperature T_a, which for different preparations is between 600 K and 800 K, maintaining the H_2S background. When the sample is cooled down to room temperature, the H_2S valve is shut.

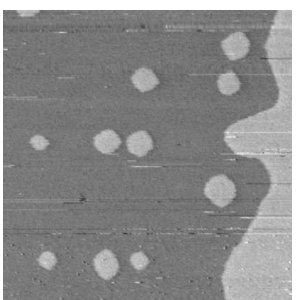

5.3 In situ HDS of C_4H_4S on MoS_2 crystallites

The first aim was to learn whether this catalytic system would be a suitable subject for investigation with the ReactorSTM. As mentioned in the introduction to this chapter, it was decided to first perform this experiment on the ReactorSTM Mark I, to discover the effects of H_2S and thiophene on the ultrahigh vacuum system. In addition, a study of the behavior of the STM itself, under reaction conditions for this catalyst, could be done. Also the capability of the STM to image the MoS_2 nano-crystallites, as well as the fact whether we could obtain a measurable reaction rate with the mass spectrometer, could be studied. Since the results of the pilot study on the ReactorSTM Mark I proved to be positive, the step to the ReactorSTM Mark II was taken. The results obtained by both STM's are mixed throughout the following sections. The first section describes the findings on the chemical composition of the crystal, using Auger electron spectroscopy. The section covering the reaction kinetics is followed by the section which finishes with an in-depth discussion about the structure of the catalyst.

5.3.1 Auger electron spectroscopy

Auger electron spectroscopy (AES) provides information about the amount of certain chemical elements present on a surface. By performing AES on our crystal, the chemical composition of the sample, before and after preparation of the MoS_2 crystallites on the Au(111) surface, and before and after exposure to reaction conditions, could be determined. Figure 5.9 shows four Auger spectra obtained in four different situations. Graph 5.9 A shows the spectrum for clean Au(111). 5.9 B shows Au(111), with MoS_2 evaporated onto it, which has not been exposed to C_4H_4S/H_2. 5.9 C shows Au(111)/MoS_2 after exposure to reaction conditions. 5.9 D shows Au(111) without MoS_2, after exposure to the reactants. And finally, 5.9 E shows the gold surface onto which an excess of molybdenum has been evaporated.

The gold peak at 69 eV was observed in all spectra, which has been used to verify whether the sample has been placed in the electron beam. Apart from this, there are various differences between the spectra in figure 5.9. The clean surface, shown in spectrum A, does not have any other peaks but the gold peak. Spectra B, C, and D all exhibit sulphur peaks at 152 eV. In spectrum B, the sulphur signal is very weak, whereas the peaks in spectra C and D are strongly pronounced. The sulphur peak in spectrum B comes only

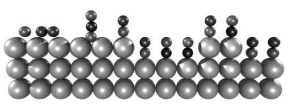

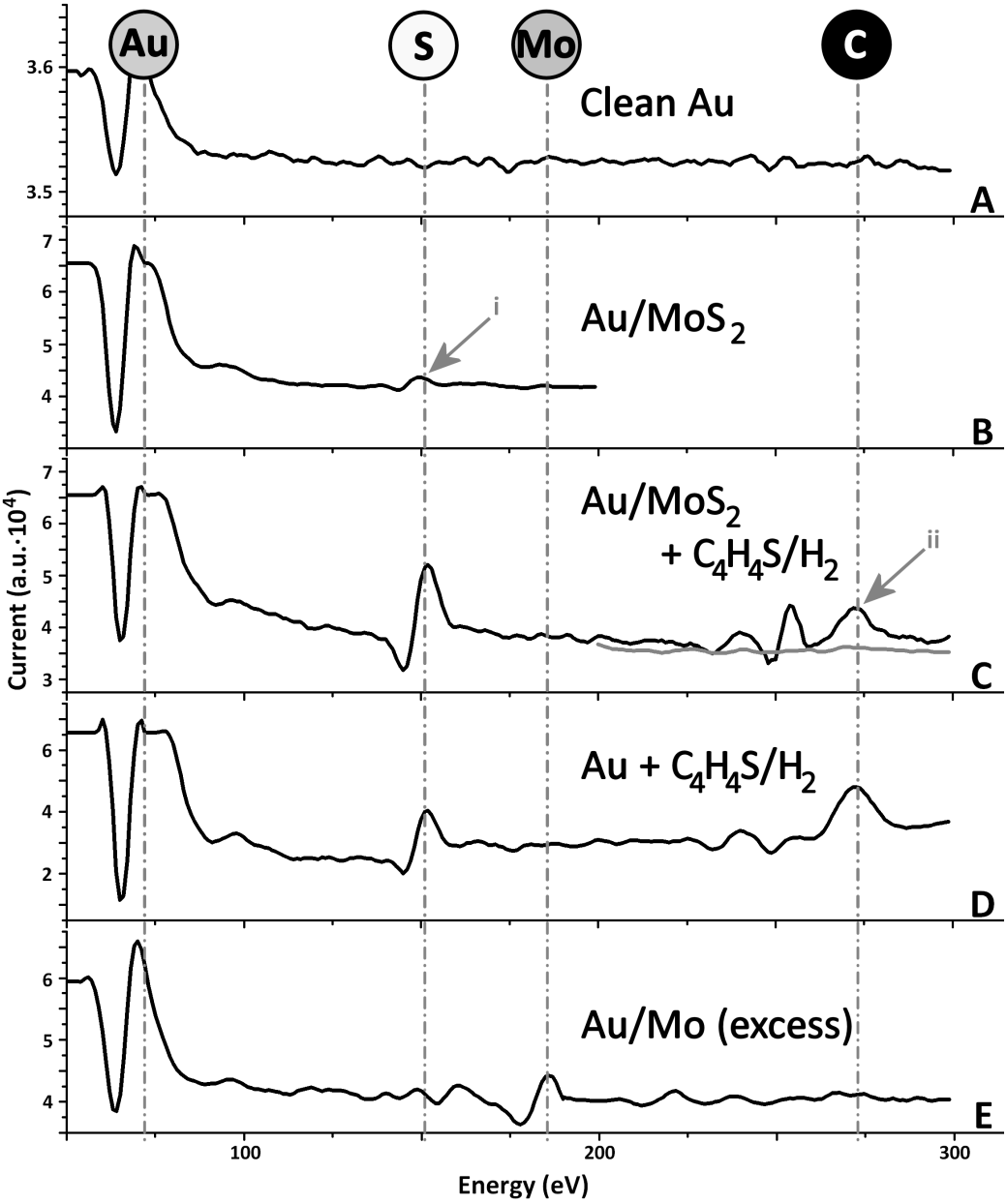

Figure 5.9: Auger spectra of Au/MoS_2 in the following situations: (A) Clean Au(111), (B) MoS_2 evaporated onto Au(111), (C) Au/MoS_2 after C_4H_4S/H_2 exposure, (D) Au(111) after C_4H_4S/H_2 exposure, (E) Excess molybdenum deposition ($\approx$ 1 ML). The peaks used for identification are 69 eV (Au), 152 eV (S), 186 eV (Mo), and 272 eV (C)

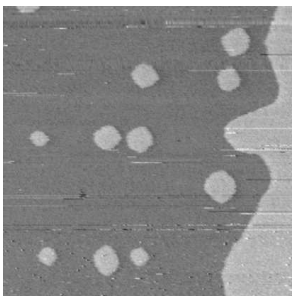

from the MoS_2 crystallites, since the crystal has not been exposed to reaction conditions. In spectra C and D, the surface has been exposed to 1.2 bar of thiophene and hydrogen/argon at 120℃. After exposure, thiophene remains on the gold surface, which can be either adsorbed or condensed – the crystal is cooled down to room temperature, prior to a transfer to the AES. In addition, spectra C and D also exhibit carbon peaks at 272 eV, indicating the presence of a carbon containing species, which could be thiophene. The carbon peak in spectrum C, however, shows a different kind of behavior than the one in spectrum D. When the bare gold surface is exposed to thiophene (D), the carbon peak is stable, whereas the carbon peak seems to disappear after the initial Auger scan of the surface, which had been catalytically active (C). The reason for the disappearance of the carbon peak in spectrum C is not exactly known. It could possibly be ascribed to a process of diffusion and reaction, under the influence of the electron beam, but this hypothesis needs verification. The only spectrum in which a clear molybdenum peak can be seen is spectrum E, in which the sample was exposed to an excess of molybdenum, with respect to the amount aimed for in the desulphurization experiments. With the quartz crystal monitor calibrated for molybdenum, it was determined that, for a full monolayer of molybdenum, an evaporation time t_e (see fig. 5.8) of 3 minutes would be needed. In the case of spectrum E, the evaporation lasted for 1 minute, leading to 1/3 Mo coverage. For these experiments, however, the coverage aimed at was between 5 and 10 %, which translated into an evaporation time between 10 and 20 seconds. In this case, the molybdenum peak at 186 eV was sufficiently low to disappear into the background noise.

5.3.2 Reaction kinetics

The adjustments applied to the ReactorSTM^{TM}, as described in section 5.2, allowed a mixture of argon, hydrogen, and thiophene to be offered to the catalytic surface in the reactor. During an experiment, the direct leak from the Kalrez seal to the UHV for residual gas analysis, with the QMS (chapter 1), was used. The amount of hydrogen offered to the surface is easy to control, by altering the ratio between the mass flow controller settings for argon and hydrogen. The amount of thiophene is difficult to adjust during an experiment. To carry this out, the vapor pressure should be increased, which is only possible by changing the temperature of the heat bath, which is a slow process. In practice, thiophene is the limiting factor for the reaction rate in the reactor; even bubbling the smallest possible amount of hydrogen, set by the gas manifold, through the thiophene initiated no decrease of reaction product yield. Because of this, and the low reaction rate, it was difficult

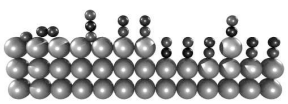

to conclude, from a flow experiment, whether the surface was catalytically active or not. Therefore, a batch experiment was performed, by closing the inlet and exhaust valve to the reactor at a set ratio of $Ar/H_2/C_4H_4S$, at a temperature of 120℃, and a pressure of 1.2 bar. In a batch experiment, it was expected that the leak of the reaction products would have a different time evolution than those of the reactants, because the reactants were being consumed, whereas the products were being produced. In addition to this experiment, a batch control experiment was performed, using the same settings, but exposing the reactant mixture to a clean Au(111) surface, without MoS_2 crystallites evaporated onto it. The outcome of both experiments are shown in figure 5.10.

Panel A, in figure 5.10, shows the evolution in time of reactants and reaction products, for the batch experiment with MoS_2 crystallites on the surface, whereas the panel B represents the control experiment. The bluish lines correspond to the reactants, hydrogen (amu 2), and thiophene (consisting of amu 45, 58, and 84). The reddish lines reflect the reaction products: H_2S (amu 34), butane (amu 29, 43, and 58), and butene (amu 41 and amu 56 (not checked)). Mass 58 corresponds both to a reactant and a product, and is green; mass 20, corresponding to doubly ionized argon, is inert and grey. The first difference between these two graphs is the level of the reaction products, which, in the upper panel, are order(s) of magnitude higher than in the control experiment, whereas the thiophene signals are more or less in the same range. There is, however, a large difference in the level of hydrogen between the two experiments. But in the control experiment, there was still an excess of hydrogen with respect to thiophene, and as mentioned earlier, hydrogen is not the limiting factor in these experiments. Secondly, as can be seen in the upper panel, the slopes of the masses corresponding to butane seem to be different from the slopes of the masses corresponding to thiophene. In the control experiment, in the lower panel, this effect cannot be seen – here the differences in slopes seem only marginal, and could be ascribed to the fact that each type of molecule has a different leak rate into the vacuum system. Moreover, the graphs with the lowest levels approach the detection limit of the mass spectrometer, which can be translated into the large variations in the measured signals. An effort to approach the difference in slopes more qualitatively, in both the real and the control experiment, is discussed in the next paragraph.

To determine the reactivity of the catalyst, it is necessary to know whether the ratios between the QMS signals are changing in time. During the batch experiment, in addition to a reaction taking place, the reactor was also being

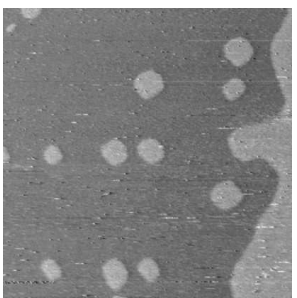

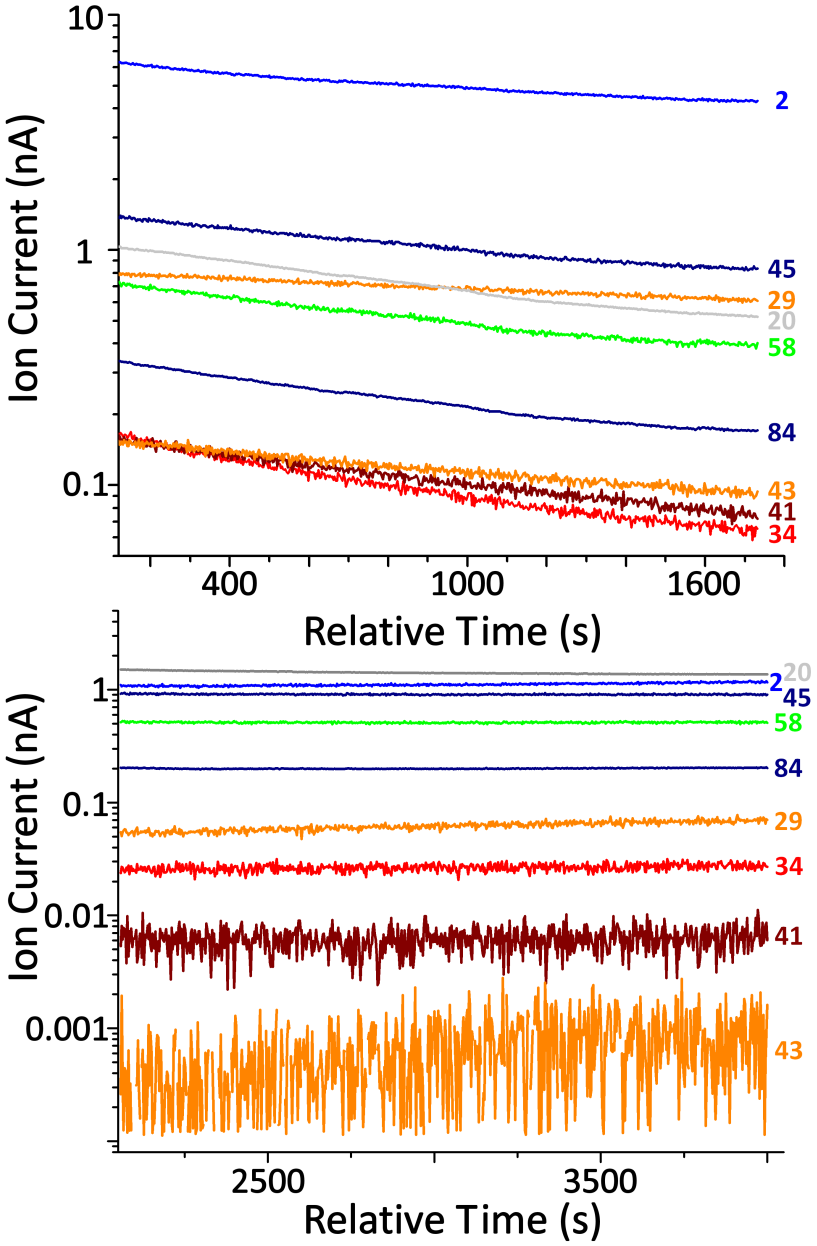

Figure 5.10: (Upper panel) The batch experiment, in which the MoS_2 islands on a Au(111) support were exposed to a mixture of argon, hydrogen, and thiophene. (Lower panel) The batch experiment, in which a clean Au(111) surface was exposed to the same reactant composition. Both experiments were performed at $T = 120℃$ and $p = 1.2$ bar.

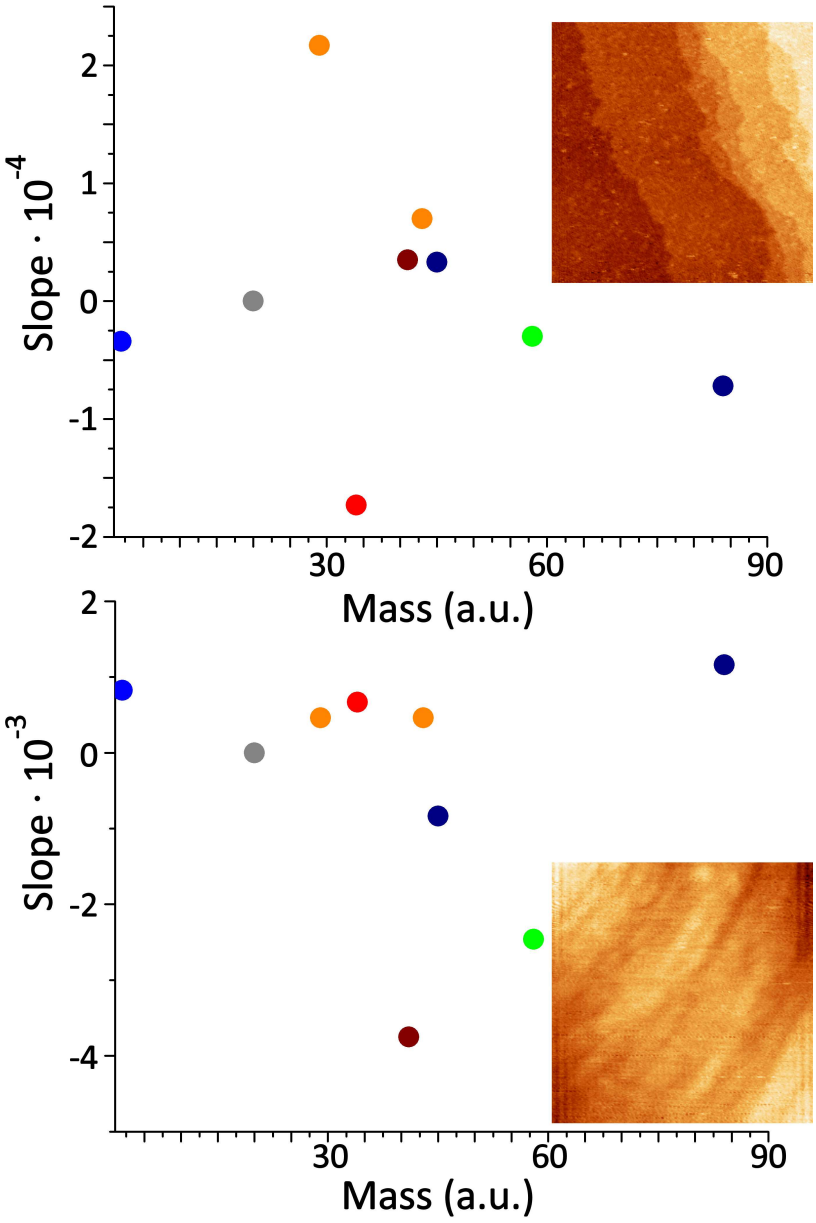

Figure 5.11: (Upper panel) The slopes of the QMS signals in the real experiment, corrected to the argon slope. The STM image is 100x100 nm^2, with $V_b = -80$ mV, and $I_t = 0.15$ nA. (Lower panel) The slopes of the QMS signals in the control experiment, corrected to argon slope. The STM image is 100x100 nm^2, with $V_b = 80$ mV, and $I_t = 0.2$ nA.

slowly emptied, via the small leak into the UHV system, for which a correction must be made. Starting from a small example: suppose there are

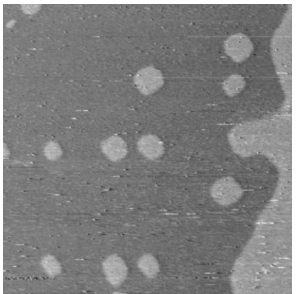

two gases, A and B, in a volume with a ratio of A:B = 1:10. If no reaction between A and B is taking place, for each molecule of A leaving the volume, 10 molecules of B will leave the volume. The time evolution of gas A and B, on a linear scale, will therefore be different. On a logarithmic scale, however, the slopes of A and B will be the same. So the first step in determining the differences between the slopes in this experiment, was to fit an exponential function to the QMS signals, to plot these functions on a logarithmic scale, and to determine the slopes of the lines resulting from this operation. Next, in this experiment, there is a carrier gas, argon, which is not participating in the reaction. The slope of argon, therefore, should be 0 if there was no leak. To correct for the leak, the values of the slopes of all the mass spectrometer signals were subtracted from the value of the slope of the argon signal. If the outcome of this simple calculation for a certain signal is negative, it means that more of this specific material is disappearing than is leaking out, meaning that this material is being consumed. On the other hand, when the outcome is positive, more material is leaking out than should happen, meaning that this material is being created in the reactor. This operation has been done, on both the real and the control experiment, of which the results are shown in figure 5.11. The color codes correspond with those used in figure 5.10. Panel A again reflects the experiment in which the catalyst is used; panel B matches the control experiment. A general look at these graphs indicates that, in the upper panel, the reaction products corresponding to butane indeed have larger slopes, when compared to the signals corresponding to thiophene, whereas the slopes are more or less the same in the control experiment. This supports the findings discussed in the last paragraph. However, there are several question marks here. During the experiment, H_2S seems to have been consumed, rather than produced – perhaps the fact that H_2S was used to create the MoS_2 crystallites compromises this signal, since H_2S is probably spread throughout the system. The marginal addition of the H_2S, created during the reaction, cannot nearly compensate for the H_2S, degassing from the walls and being evacuated by the pumps. Also, despite the fact that thiophene had a negative slope, its ionized mass 45 had a positive slope; this was reversed in the control experiment. In addition, the signal of mass 45 was higher than the signal of mass 84 (see fig. 5.10); of all the substances used, the only combination of atoms adding up to 45 was S=C-H^+, which could only have originated from thiophene. An explanation for this is not yet available.

In the upper right hand corner of both graphs, in figure 5.11, an STM image obtained by the ReactorSTM Mark I, corresponding to the situation of that particular experiment, is shown. Although the image quality is poor,

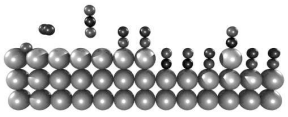

it can clearly be seen that, in the case of the catalytically active surface, there are small MoS_2 crystallites dispersed over the surface. In the case of the control experiment, the surface is not covered with these nano-particles.

5.4 Catalyst structure and reactivity: Experimental

In the initial study, performed on the ReactorSTM Mark I, several of the aspects described in section 5.1.1 were observed. As argued in section 5.1.2, Au(111) was chosen as a support for the MoS_2 nano-crystallites; figures 5.12 and 5.14 show the STM images we obtained under vacuum conditions[7]. Figure 5.12 shows the effect of the bias voltage on the apparent height of the MoS_2 crystallites. For type I crystallites, the apparent height asymptotically approached a value of 3.0 Å at large bias voltages, starting from very small heights at small bias voltages. This effect has been ascribed to the interaction of the crystallites with the Au(111) substrate. The semiconducting properties of the crystallites, in this situation, were slightly influenced, leading to a change in the band gap to -1 V. Tunneling within this band gap gave mixed Au/MoS_2 states, which at low bias voltages were dominated by the gold substrate. When the bias voltage was gradually increased, more states of the crystallites became available for tunneling, due to the integration of the state density, increasing the apparent height of the crystallites in the STM images. Outside the band gap, the electronic structure was dominated by the MoS_2 crystallites, translating into an apparent height of 3.0 Å, approaching the real height of a S-Mo-S slab of 3.16 Å. Image 5.12 A was obtained with a bias voltage of -80 mV. From the STM image and the corresponding height profile a, it can be seen that the MoS_2 crystallite, indicated by the hatched area, barely stands out, with respect to the gold layer below. In comparison, image 5.12 B was recorded with a bias voltage of -1.9 V. The matching height profile b shows that the apparent height of the MoS_2, in the profile again corresponding to the hatched areas, is now 2 Å, approaching the value of a single S-Mo-S slab [143].

A second effect, which has been observed and used to characterize the

[7]Actually the "vacuum conditions" comprised a $p <\sim 10^{-4}$ mbar of mainly H_2 exposure, since the volume of the reactor, during STM measurements, was not evacuated, and the main residual gas was H_2. This already translates into a slight morphological change of the MoS_2 crystals, from triangular into deformed hexagonal, as can be seen in figure 5.14 D and F; this will be discussed at a later stage in this section

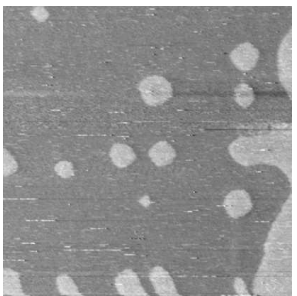

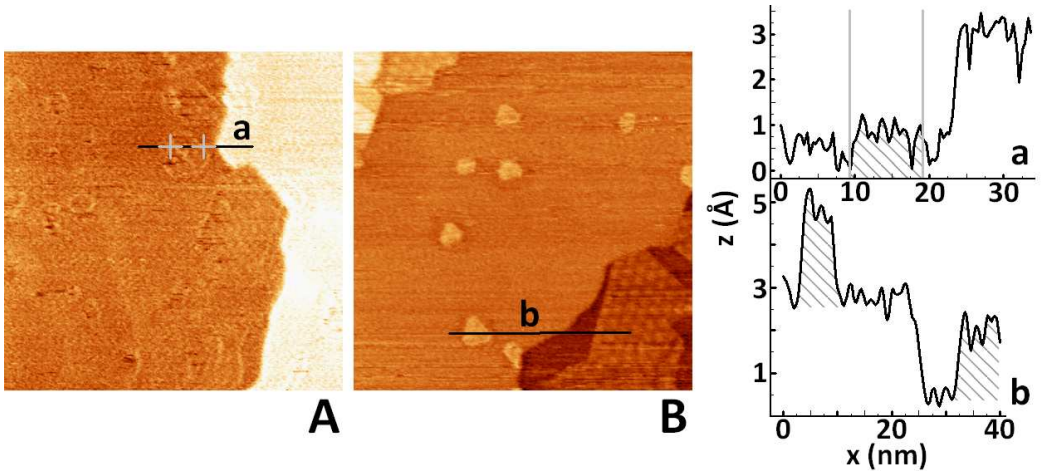

Figure 5.12: Two 100 x 100 nm^2 STM images of MoS_2 on Au(111). For image A, $V_{bias} = -80$ mV, $I_t = 0.2$ nA; for image B, $V_{bias} = -1.9$ V, $I_t = 0.15$ nA.

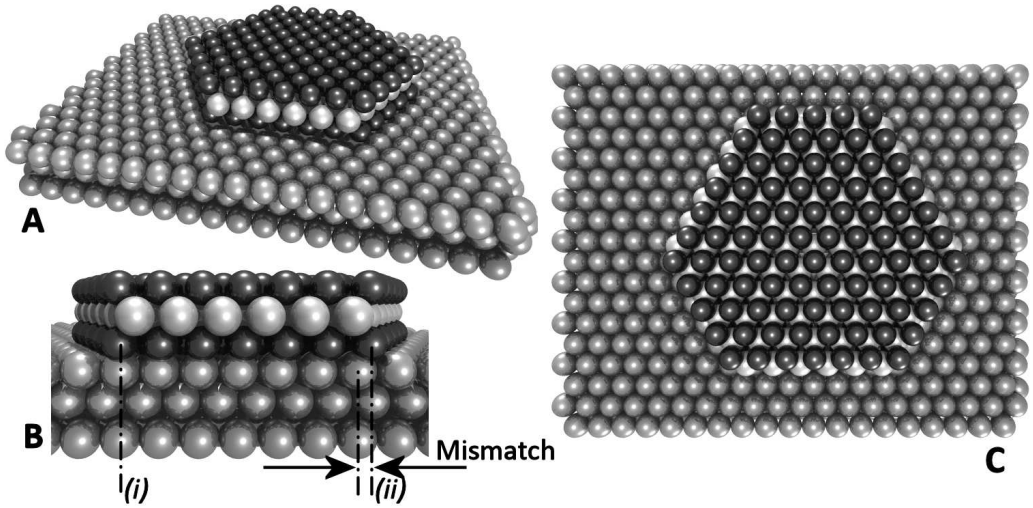

Figure 5.13: (A) A 3D impression of a MoS_2 crystallite on a gold (111) substrate. (B) A side view of image (A), showing the difference in lattice spacing between the crystallites and the substrate from which the Moiré pattern originates, indicated as "mismatch". (C) A top view of image (A).

MoS_2 crystallites with the ReactorSTM Mark I, was the sintering and accumulation of MoS_2 at the Au(111) steps, occurring at higher annealing temperatures T_a, as shown in figure 5.14. Since the resolution of the ReactorSTM Mark I was insufficient to atomically resolve 10 to 20 Å wide MoS_2 crystallites, a $T_a \approx 800$ K was used, in order to create these larger crystallites. Since the interatomic distances of unreconstructed Au(111) (2.88 Å),

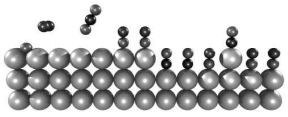

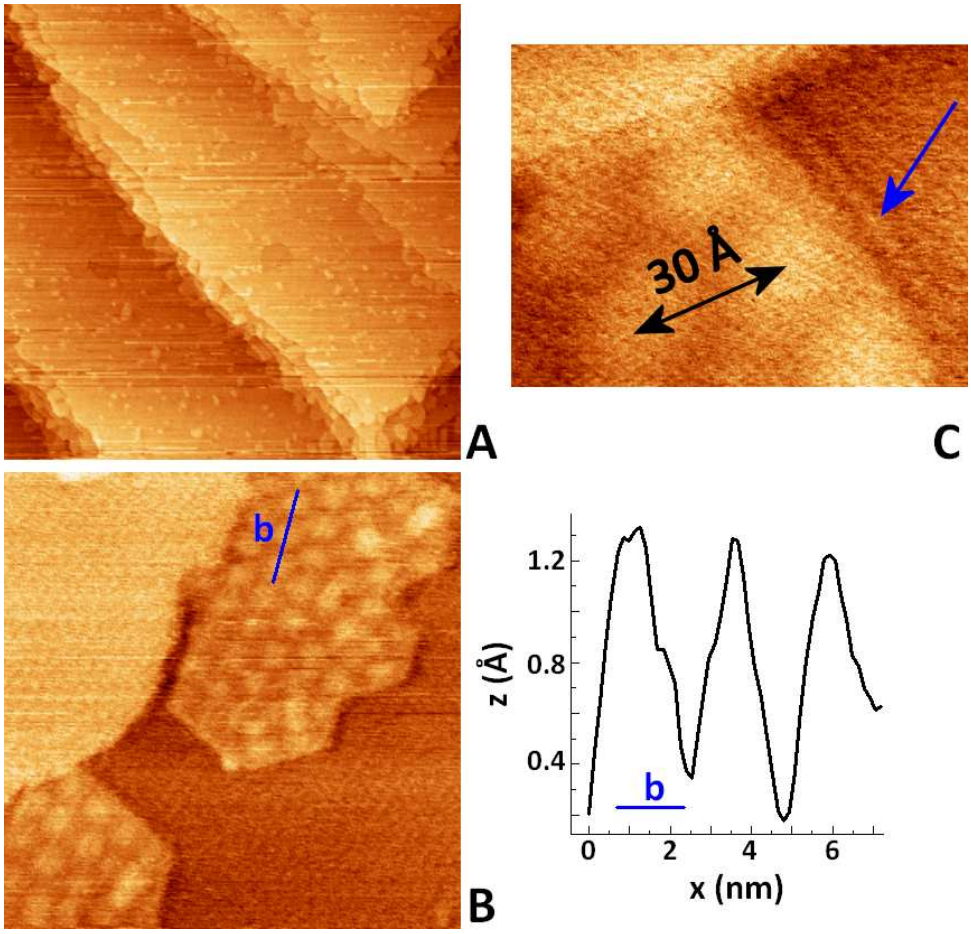

Figure 5.14: (A) A 400 x 400 nm^2 STM image of Au(111), with MoS_2 crystallites on it. (B) A 35 x 35 nm^2 STM image. Corresponding height profile (b) shows the corrugation of the Moiré pattern. (C) A 10 x 10 nm^2 STM image, in which the edge states of the crystallites can be seen. The periodicity of the Moiré pattern is 30Å. All STM images in this figure were obtained at $V_b = -1.9$ V and $I_t = 0.15$ nA.

which was believed to support the crystallites [145], and MoS_2 (3.15 Å) differ, a Moiré pattern should appear, due to the lattice mismatch. The lattice mismatch is shown schematically in the ball models in figure 5.13. (A) shows an on scale 3D impression of a MoS_2 crystallite on Au(111), for which a side view and top view are shown in 5.13 B and C. In the side view, the lattice mismatch, leading to the Moiré pattern between Au and MoS_2 is indicated by the arrows. Three STM images are shown in figure 5.14, which were obtained at room temperature and under exposure to the residual gases in the reactor,

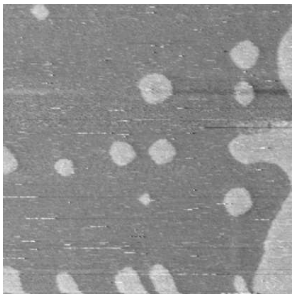

which was not being evacuated during the STM operation. Image 5.14 A is a large scale scan, showing both sintered MoS_2 crystallites, collected at the Au(111) steps, and 10 to 20 Å MoS_2 nano-particles, scattered on the gold terraces. The small scale images 5.14 B and C, and also figure 5.12 B, reveal more detailed information about the MoS_2 structure. The nano-crystallites on the terraces, as visible in image 5.12 B, exhibited a deformed hexagonal structure, ascribable to the reducing conditions in the reactor volume (see footnote 7); the residual gas consisted mainly of hydrogen. The height of the crystallites, indicated in the corresponding height profile in figure 5.12 b, was 2 Å, corresponding to a single S-Mo-S slab. Furthermore, the bright rim along the edges of the nano-crystallites was slightly visible, although it was difficult to distinguish in individual height profiles. In image 5.14 C, the bright rim along the edge is more clearly distinguishable, and is pointed out by the blue arrow. The larger MoS_2 patches, shown in images 5.14 B and C, clearly exhibit an overlayer structure, with a periodicity of 30 Å. The z-corrugation of this corrugation is about 1 Å, which can be seen in the height profile b, corresponding to figure 5.14 B. For a non-rotated hexagonal overlayer – the MoS_2 overlayer is not rotated with respect to the gold substrate – with lattice constant a_o on a hexagonal substrate with lattice constant a_s, a buckling would be expected, due to the atoms of the overlayer structure alternatingly being positioned at on-top sites and high-coordination sites. This buckling would have a periodicity of $a_s \cdot a_o/(a_o - a_s)$ [186]. For $a_o = 3.15$ Å and $a_s = 2.88$ Å, this leads to a periodicity of 33.6 Å, which corresponds well with the distance measured between the maxima of the Moiré pattern, indicating that the structures observed in the STM images are MoS_2 crystallites.

However, as can be clearly seen in the STM images in figure 5.12 B and 5.14 B, and as mentioned in footnote 7, the shape of the crystallites on the Au(111) terraces is not triangular, but deformed hexagonal. The question of what happens under reaction conditions needs to be addressed, since the gas composition in the reactor of the STM, during a "vacuum" experiment, consisted mainly of hydrogen, one of the reactants in the hydrodesulphurization process. Despite the fact that the research reported in the literature ([145, 160, 175, 177, 179–181]) has not been performed under reaction conditions, the experimental studies include investigations of the interaction of MoS_2 crystallites with hydrogen and thiophene separately, and the theoretical DFT studies elaborate on the morphology and edge terminations, under practical HDS (reducing) conditions. These studies, as described in section 5.1.1, reveal a complex interplay between the different aspects of the reaction mechanism, and the crystallites' morphology, under different environmen-

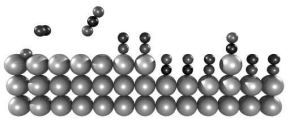

tal conditions. The effect on the reactivity and reaction mechanism of the changing edge termination, under the influence of the size of the crystallites, is unknown. Also, the experimental studies have not been performed in situ under reaction conditions. In addition, a change in the chemical potential is predicted, by density functional theory, to change the active sites and the structure of MoS_2 [160]. In summary, this theoretical study investigated the effect of the sulphur chemical potential μ_S on the sulphur saturation of the Mo and S edges of MoS_2 crystallites. For the Mo terminated edge, in the physically realistic range, the S coverage is expected to be 50 %; only at a very high μ_S will there be 100 % coverage. Sulphur coverage of < 50 % is only stable outside the physically realistic range of μ_S. For the S terminated edge, 100 % coverage is expected, in the realistic range for μ_S; formation of S vacancies will only occur at low values of μ_S. Sulphur exchange between the edges might occur in this situation. The absence of experimental studies, under realistic conditions, in combination with theoretical studies predicting differences in catalytically active sites, between vacuum and high-pressure conditions, confirms the importance of studying this reaction system in situ, under reaction conditions, which was the target with the ReactorSTM. During the first runs of this experiment on the ReactorSTM Mark I, knowledge of whether the reaction system was suitable for study with this type of machine was required. The STM images, obtained by the ReactorSTM Mark I, resolved the MoS_2 crystallites on the Au(111) surface, as shown in figure 5.14. The batch experiment, as described in section 5.3.2, indicated a measurable catalytic activity of the surface. Together, they have proven the suitability of the ReactorSTM for this catalytic system. In addition, the H_2S and thiophene, necessary for sample preparation and desulphurization experiments, did not prove to become a serious handicap for the ultrahigh vacuum system. There remained, however, a major issue with respect to the experiment: under reaction conditions, the tip approach was very unreliable. On many occasions, the tip did not detect a tunneling current, i.e. it either got stuck or the apex was covered by some insulating layer. And in most of the few cases when the tip did find the surface, a tip crash occurred. One of the possible explanations is the presence of a cold spot in the reactor; as described in section 5.2, an external heating cartridge was used for heating up the reactor, which, due to its position and the low thermal conductivity of stainless steel, might not be able to heat up all parts of the reactor equally. Thiophene might condense onto a cold spot (in which "cold" means below 84℃) on the tip holder or the tracks along which the tip holder slides, affecting the properties of the approach motor. Perhaps the acceleration required to make the tip holder perform its stick-slip motions exceeded the maximum acceleration provided by the piezo element. Another possibility is

the presence of sulphur-containing molecules covering the tip apex, making it electrically insulating. Additionally, the resolution of the ReactorSTM Mark I, under reaction conditions, was too poor to atomically resolve the crystallites, edge vacancies, and the large organic molecules adsorbed onto the Mo and/or S edges; the edges would also be hard to distinguish.

All in all, the pilot experiment performed on the ReactorSTM Mark I was successful in imaging and detecting reactivity, however, with poor resolution and unreliable tip approach. Both the success, as well as the drawbacks, lead to repeating the experiment with the ReactorSTM Mark II, in which it was hoped to observe the dynamics of the morphology of the crystallites, under reaction conditions, as well as the various reaction steps. An attempt to solve the approach issue by heating up the whole SPM chamber to 110℃ during STM operation was made. The initial findings are summarized in figure 5.15. Image A and B show the clean gold surface, A on a large scale, showing the herringbone reconstruction, and B on the atomic level. The reconstruction on the Au(111) surface originates from the reduced coordination number of the surface atoms, which are compressed by about 5 % along the $1\bar{1}0$ direction. This leads to two different domains, an fcc domain, and an hcp domain along the $11\bar{2}$ direction. These domains are separated by the gold atoms near the bridge positions of the bulk layer below, which appear as bright lines in the STM image. The reconstruction has a $22\text{x}\sqrt{3}$ unit cell. On a larger scale, these domains exhibit a zigzag pattern, with angles of 120°, due to elastic interactions. This zigzag pattern resembles a fish scale, hence the name "herringbone" reconstruction [145, 161, 162]. Image C, in figure 5.15, shows the gold surface when more then a monolayer of molybdenum is deposited. The surface is characterized by blobs, which seem to have a preference for buckling at the steps. From the height profile *c* can be seen that the difference in height between two terraces is 6 Å, which does not correspond to any integer, multiplied by the monatomic step height of Au(111)[8], but does correspond to a multiple step of some kind, rather then a single step. Along the steps, "speed bumps" of accumulated material exist, also with a height of 6 Å, as can be seen in the height profile. Finally, image D shows an STM image from a successful MoS_2 deposition experiment in the ReactorSTM Mark II. The quality of the image is not very high, but the characteristic Moiré pattern can be distinguished. The step height of the crystallites is 3 Å, as can be seen in height profile *d*. Although MoS_2 crystallites have been successfully created in this experiment, the recipe has not yet been optimized. The small

[8]This might arise under the influence of Au-Mo alloying, which is discussed in the appendix at the end of this chapter

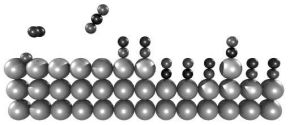

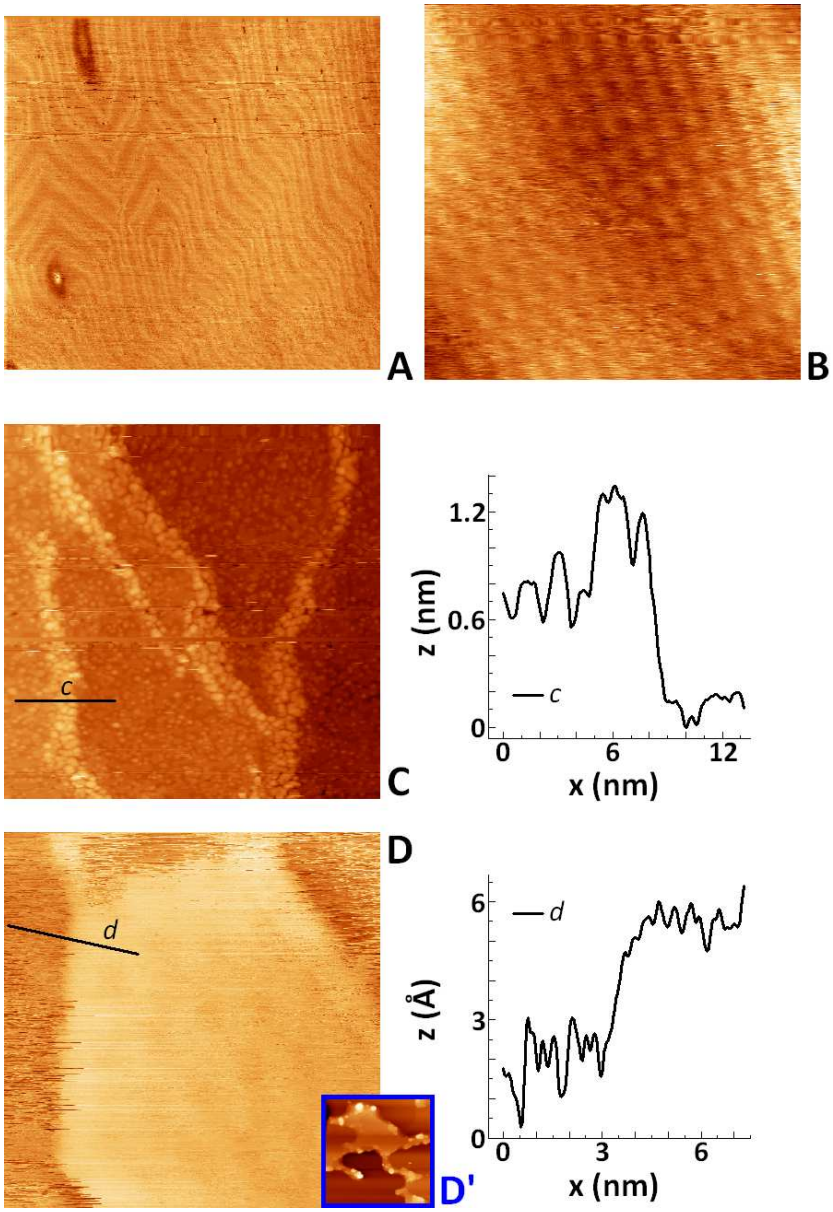

Figure 5.15: STM images obtained by ReactorSTM Mark II. (A) A 100 nm^2 STM image, showing a large terrace on Au(111), exhibiting the herringbone reconstruction. (B) A 2.5 nm^2 STM image of atomically resolved Au(111). (C) A 25 nm^2 STM image of Au(111) with > 1 monolayer of Mo deposited; c is the corresponding height profile. (D) A 10 nm^2 STM image of a MoS_2 crystallite on Au(111), with height profile d. Image D' is a 110 nm^2 subsection from a large scan, showing the accumulation of MoS_2 islands at the steps.

image, shown in figure 5.15 D', is a cut-out from a large scale image, showing that, all the MoS_2 crystallites are on the edges of the Au(111) terraces, and on the terraces themselves no nano-particles can be seen. Unfortunately, it has not been possible to continue with this experiment up to the moment of writing, after obtaining the series of STM images, including figure 5.15. This means that the aim of atomically resolving the MoS_2 crystallites, and of performing high-pressure experiments lie in the near future [163].

Although the focus of this study has only been on the unpromoted MoS_2 nano-crystallites, a few words should be included about the addition of the main promoters for MoS_2, cobalt and nickel. Adding cobalt or nickel to the catalyst, on its industrial support γ-alumina, the promoter can appear in three forms. Firstly, the promoter atoms can dissolve into the γ-alumina, and secondly, cobalt can form a stable sulphide, Co_8S_9, on top of the support. Neither of these forms are believed to influence the desulphurization reaction rate. The third form, in which cobalt or nickel atoms replace some of the molybdenum atoms in MoS_2, forming CoMoS or NiMoS, increases reactivity by an order of magnitude. It is believed that the promoter atoms, in this structure, do not affect the molybdenum edges; they do, however, replace the molybdenum atoms at the sulphur edges. The activation energy for the creation of a sulphur vacancy, in the case of a sulphur edge, in which the metal atoms are replaced by cobalt or nickel, is significantly lower than for the sulphur edge with molybdenum [140, 187, 188]. In future experiments, adding these promoters to the MoS_2 crystallites has been planned, to study their influence on the activity of the catalyst under realistic conditions.

5.5 Concluding remarks

In conclusion, two milestones have been achieved in this experiment, up to the moment of writing. Firstly, it has been possible to successfully deposit MoS_2 nano-crystallites onto a Au(111) support, both with the ReactorSTM Mark I and Mark II. Up to now, in both cases it has only been possible to characterize the crystallites by the Moiré pattern, generated due to the lattice mismatch between Au(111) and MoS_2. However, the ReactorSTM Mark II is capable of atomically resolving the Au(111) surface, which opens the possibility of also atomically resolving the crystallites. This would be impossible with the ReactorSTM Mark I. Secondly, the activity of the catalyst under high-pressure and high-temperature conditions has been shown, with the combination of a batch experiment and a control experiment, using the

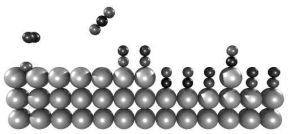

ReactorSTM Mark I. The microscope was also able to image the catalyst under these conditions, however with poor quality.

Further research is necessary, to investigate the behavior of the catalyst under high-pressure conditions, e.g. to determine which of the two edge terminations will be dominant, and what the role of each of the edges is, during various reaction steps. In a later stage, also the effect of the promoters cobalt and nickel should also be studied in the same fashion.

Appendix: Mo-Au alloying

At the first attempts at preparing molybdenum disulfide adatom islands on the (111) surface of gold, an unexpected, but easy to explain behavior was observed. Figure 5.16 shows a series of STM images, under different conditions. Image A and B are an example of what the STM images looked like, after the first MoS_2 deposition attempts. As can be seen, adatom island structures are present at the surface, which at first suggested the presence of MoS_2 on the surface. However, these surfaces were not stable, but began to behave like the series of STM images shown in figure 5.17. This figure shows four consecutive STM images A to D, each with a recording time of about 80 s. The markers I and II follow two evolving steps on the gold surface, throughout the imaging. As can be seen, these steps change drastically within the recording time of these four images, in total about five minutes, indicating a huge mobility of the steps on the gold surface. The density of adatom islands has significantly decreased, with respect to image A and B in figure 5.16; in the lower left hand corner of the images, some adatom island features still can be seen, which exhibit a larger stability than the steps on the gold surface. Apparently these are not MoS_2 crystallites (or at least stable ones) in image A and B of figure 5.16. There are a few indications supporting this hypothesis. Firstly, as the height profile a_2 on image A suggests, the apparent height of the adatom structures is 2 Å, which means these structures in this case actually *cannot* be MoS_2. This is because the bias voltage used to obtain this image, 80 mV, is well below the band gap of the semiconducting crystallites, in which case it should yield a very low apparent height for the crystallites, as in figure 5.12 A. The step height of the terraces, as indicated in the height profile a_1, is about 2.5 Å, which does seem to be different from the adatom structure's height. Next to the very irregular shapes of the adatom structures in image B, which according to the height profile b seem to exhibit the same step height as the terraces, vacancy islands can also be distinguished. As a reference, image C in figure

5.16 shows an STM image of one of the successful deposition experiments, exhibiting large MoS_2 crystallites, which are recognizable from their characteristic Moiré pattern. The step height of the Au(111) terrace here is 2.3 Å; the apparent height of the crystallites in this experiment were measured to be 2 Å, as shown in figures 5.12 and 5.14. Furthermore, in this case, no mobility of the Au(111) steps was observed. Image D in figure 5.16 shows the freshly prepared Au(111) surface, before Mo/H_2S exposure, in which the step height of the terraces again is 2.5 Å. In all these images, the step heights of the terraces correspond to a single step on Au(111). This is also the case for the steps in image A of figure 5.17, as shown in its corresponding height profile *a*. Finally, it should be mentioned that, in the situation of image A and B of figure 5.16, molybdenum, in combination with sulphur, (probably) was not deposited on the Au(111) surface. Whenever we observed the high step mobility, only a large series of sputtering and annealing cycles[9] would completely remove this mobile step behavior, returning to the initial situation of a clean Au(111) surface.

So since there has been material deposited on the gold surface, leading to a high step mobility, the question arises as to what mechanism is behind it. The literature reports the possibility of molybdenum alloying with gold. When molybdenum is deposited on gold, it forms clusters in the elbows of the herringbone reconstruction. This structure is stable up to a temperature of 600 K, above which gold encapsulates the molybdenum, forming Au-Mo-Au sandwiches on the surface. The same happens when molybdenum is deposited at a temperature above 525 K (one paper reports already having observed alloying at a deposition temperature of 300 K). When the alloying takes place, a large mobility of the steps on the gold surface has been observed. Once alloyed, exposure to atomic oxygen or sulfur can separate the metals, ending with molybdenum oxides or sulfides on top of the surface [189–191].

What has apparently been seen, in the early experiments here, is this alloying between the two metals, because the initially observed adatom islands (which could be just molybdenum, or molybdenum in combination with some sulphur), disappear; thereafter, huge step mobility on the gold surface was observed. There are two possible reasons for this alloying to occur in this case. In the initial deposition experiments, various parameters were being tuned, including H_2S pressure, molybdenum, and H_2S exposure time,

[9] On the order of ten cycles were needed to get rid of the step mobility. Molybdenum is hard to get rid of.

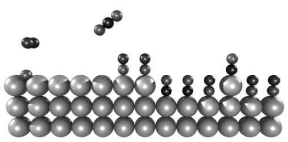

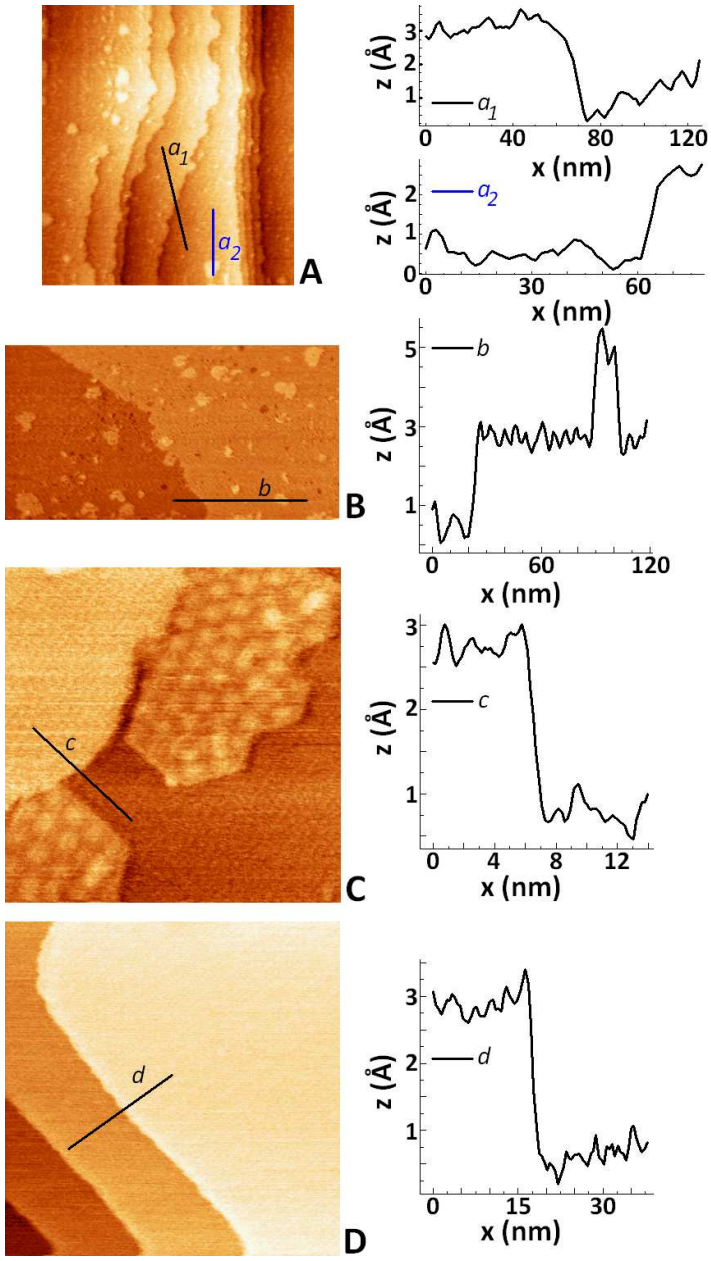

Figure 5.16: (A) A 300 x 335 nm^2 STM image, with height profiles a_1 and a_2, showing adatom island structures on Au(111); V_b = 80 mV; I_t = 0.2 nA. (B) A 300 x 155 nm^2 STM image, with height profile b; V_b = -2 V, I_t = 0.2 nA. (C) A 35 nm^2 STM image, with height profile c, showing MoS_2 on Au(111); V_b = -1.9 B, I_t = 0.15 nA. (D) A 100 nm^2 STM image of terraces on Au(111); V_b = 80 mV, I_t = 0.2 nA. T = 293 K.

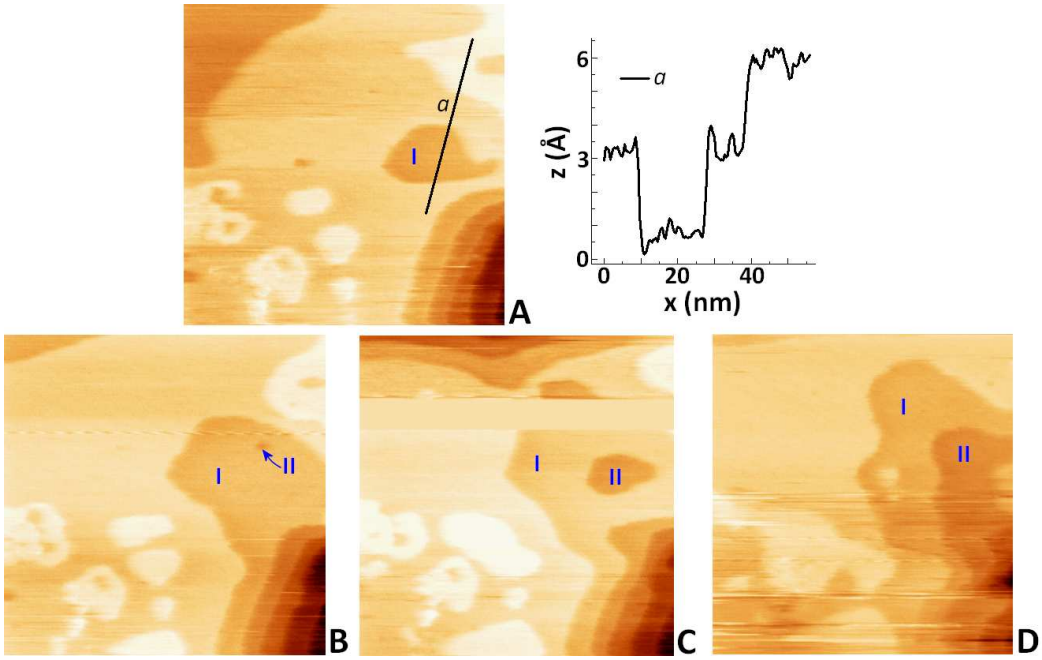

Figure 5.17: Four consecutive 100 x 100 nm^2 STM images (the recording time was ~80 s/image), showing large step mobility. The indicated terrace steps I and II have been followed. For image A, a corresponding height profile a is included. T = 393 K; V_b = -0.8 V; I_t = 0.2 nA.

and temperature. Under the "wrong" conditions this might lead to instable Mo/MoS_2 structures on the Au(111) surface, eventually leading to alloying of the two metals. However, there is one more factor present. When starting with the experiments involving thiophene, and still tweaking the parameters in the initial preparation steps, the alloying was no longer observed. This leaves a second option for destabilizing MoS_2 structures: the residual gases in the reactor, prior to thiophene exposure. The main residual gases in the reactor volume, before it was exposed to thiophene, were CO and H_2. CO does interact with MoS_2, but is not expected to destroy the islands [192]. H_2, on the other hand, reacts with the step edges, forming H_2S, which is part of the desulphurization reaction to be studied. With no organosulphur compounds present to fill these vacancies, hydrogen will proceed to react away all the sulfur, leaving bare molybdenum on gold, opening the possibility of alloying of the two metals.

Presumabely the interaction of the residual hydrogen in the reactor with the MoS_2 nano-particles is one of the key players in these experiments, in

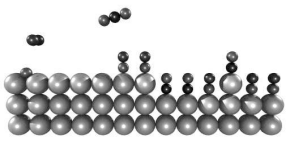

which the metals alloy. Initially, adatom islands are seen (of which, it should be said, their composition is not completely certain, due to the low bias voltage used to be able to image them, as in figure 5.16 A; it could be MoS_x, just Mo, or even Au already covering Mo). Later the fingerprint of alloying (the mobile steps) was observed. That the alloying did not take place directly, but only after an exposure of several hours in the reactor, could be explained by the fact that it takes hydrogen some time to react away all the sulfur – remember that the sample was at room temperature. Since molybdenum sulphides are stable on the gold surface, and sulphur is capable of de-alloying gold and molybdenum, a large fraction of the sulphur would have to be removed before alloying could begin. In addition, when thiophene was used, alloying was no longer observed. This could mean that when there is a steady supply of a sulphur containing carbohydrate, it fills up the vacancies created by the residual hydrogen, and the islands on the surface are stabilized. Once thiophene is in the reactor surroundings, it is very difficult to remove, and it continues to outgas. This means that, even when there is no external supply of thiophene, the remnants of the previous experiments are enough to counteract the destabilizing effect of hydrogen.